

Expand and Prune: Maximizing Trajectory Diversity for Effective GRPO in Generative Models

Shiran Ge^{1,2,*}, Chenyi Huang^{1,2,*}, Yuang Ai^{1,2}, Qihang Fan^{1,2}, Huaibo Huang^{1,†}, Ran He^{1,2}

¹MAIS & NLPR, Institute of Automation, CAS ²School of Artificial Intelligence, UCAS

Abstract

Group Relative Policy Optimization (GRPO) is a powerful technique for aligning generative models, but its effectiveness is bottlenecked by the conflict between large group sizes and prohibitive computational costs. In this work, we investigate the trade-off through empirical studies, yielding two key observations. First, we discover the reward clustering phenomenon in which many trajectories collapse toward the group-mean reward, offering limited optimization value. Second, we design a heuristic strategy named Optimal Variance Filtering (OVF), and verify that a high-variance subset of trajectories, selected by OVF can outperform the larger, unfiltered group. However, this static, post-sampling OVF approach still necessitates critical computational overhead, as it performs unnecessary sampling for trajectories that are ultimately discarded. To resolve this, we propose Pro-GRPO (Proactive GRPO), a novel dynamic framework that integrates latent feature-based trajectory pruning into the sampling process. Through the early termination of reward-clustered trajectories, Pro-GRPO reduces computational overhead. Leveraging its efficiency, Pro-GRPO employs an “Expand-and-Prune” strategy. This strategy first expands the size of initial sampling group to maximize trajectory diversity, then it applies multi-step OVF to the latents, avoiding prohibitive computational costs. Extensive experiments on both diffusion-based and flow-based models demonstrate the generality and effectiveness of our Pro-GRPO framework.

1. Introduction

Aligning visual generative models with human preferences is crucial for achieving controllable content generation [5, 15, 25]. Among various alignment techniques, reinforcement learning (RL) methods, such as PPO [34], DPO [28],

and GRPO [35], have been widely adopted [4, 12, 20, 38]. Particularly, GRPO is favored for its unique in-group sampling mechanism, which enables robust advantage estimation without the need for a trained value function [7, 42]. However, the effectiveness of GRPO relies on a large group size to ensure reliable advantage estimation [22]. This requirement imposes memory and computational burdens, forcing a suboptimal trade-off [47]: while a small group size fits resource constraints, it destabilizes advantage estimation and hampers exploration; conversely, a large group size becomes computationally prohibitive. This dilemma ultimately bottlenecks the model’s performance potential.

Delving into this trade-off, we conducted two empirical studies on GRPO’s sampling and obtained two key observations. First, we identify an reward clustering phenomenon: for a single prompt, standard GRPO generates many trajectories whose rewards concentrate near the group mean. This clustering degenerates normalized advantages, limiting the contribution of the corresponding samples to the overall optimization process, while consuming the same computational resources. Meanwhile, naive techniques like random subsampling fail to resolve this phenomenon (Fig. 1).

Second, building on the observed reward clustering, we hypothesize that such clustering could be detrimental to optimization. To validate this, we propose a simple yet effective strategy named Optimal Variance Filtering (OVF). OVF is a heuristic algorithm that selects trajectories by maximizing reward variance, strategically focusing on both high and low reward extremes. Our experiments show that OVF effectively mitigates reward clustering phenomenon and enhance optimization performance. This validates the “*Less is More*” principle, proving that a smaller, high-variance subset can outperform a larger, unfiltered group.

However, while OVF effectively filters reward-clustered trajectories to enhance optimization by maximizing reward variance, it suffers from the limitation of post-sampling filtering, which still incurs unnecessary computation for reward-clustered trajectories. To address this issue, we introduce Pro-GRPO (Proactive GRPO), a dynamic framework that prunes trajectories based on latent features dur-

* Equal Contribution.

† Corresponding author: huaibo.huang@cripac.ia.ac.cn

Emails: {shiran.ge, rhe}@nlpr.ia.ac.cn, huangchenyi2026@ia.ac.cn, {shallowdream555, fanqihang.159}@gmail.com

ing sampling. By early-terminating reward-clustered trajectories, the approach significantly improves sampling efficiency. Leveraging this efficiency, Pro-GRPO adopts the ‘‘Expand-and-Prune’’ strategy: it first expands the size of initial trajectory sampling group to maximize diversity, and then applies multi-step OVF during the generation process. This approach allows Pro-GRPO to achieve a larger trajectory diversity, and significantly improve performance, without incurring prohibitive computational costs.

In summary, our contributions are:

1. We conduct two in-depth empirical studies on GRPO’s sampling trajectories, yielding two key observations: (1) GRPO exhibits reward clustering phenomenon. (2) A high-variance subset of trajectories can outperform a larger, unfiltered sampling group.
2. We introduce the Pro-GRPO framework, which integrates a dynamic latent feature-based pruning framework enabling efficient in-process sampling. Leveraging this efficiency, we adopt an ‘‘Expand-and-Prune’’ strategy to maximize trajectory diversity without incurring prohibitive computational costs.
3. We conduct extensive experiments on both diffusion-based and flow-based generative models, demonstrating the generality and effectiveness of our Pro-GRPO framework.

2. Related Work

2.1. Diffusion and Flow Matching Models

Modern high-fidelity Text-to-Image (T2I) synthesis is primarily driven by diffusion [3, 26, 30, 31] and flow matching [8, 17, 41] models, which share the common objective of learning a continuous path from noise to data distributions [8, 10]. While diffusion models perform denoising via stochastic differential equation (SDE) solvers or discrete denoising diffusion probabilistic model (DDPM) steps, flow matching directly learns a velocity field, enabling highly efficient deterministic sampling through ordinary differential equation (ODE) steps [21]. A series of theoretical works [1, 2, 6, 10] have unified the characterization of diffusion and flow matching models under an SDE/ODE framework. This unification provides a theoretical foundation for subsequently integrating online reinforcement learning algorithms, such as GRPO, into the post-training phases of these models [18, 22, 47].

2.2. GRPO for T2I Models

GRPO has gained prominence in aligning T2I models [9, 12, 24, 39, 48, 49], with methods such as FlowGRPO [22] and DanceGRPO [47] that reformulate the generation process as an equivalent SDE, enabling stochastic policy exploration and facilitating GRPO integration into flow models. Building on these foundations, subsequent research

has refined algorithmic details such as optimizing credit assignment [13, 19] and improving reward computation [40]. However, less attention has been paid to reward clustering in sampling groups. Many trajectories concentrate near the group mean, adding little gradient signal. Pro-GRPO tackles this by latent-feature pruning with an expand-and-prune schedule, retaining a small high-variance survivor set that enhance performance without prohibitive cost.

3. Preliminaries

3.1. Diffusion Models

A diffusion model [14] specifies a forward noising process that perturbs a clean sample \mathbf{x}_1 toward Gaussian noise. At time t the noisy state is

$$\mathbf{x}_t = \alpha_t \mathbf{x}_1 + \sigma_t \boldsymbol{\epsilon}, \quad \boldsymbol{\epsilon} \sim \mathcal{N}(\mathbf{0}, \mathbf{I}), \quad (1)$$

where (α_t, σ_t) is the noise schedule. For sampling, data can be generated from a prior $\mathbf{x}_T \sim \mathcal{N}(\mathbf{0}, \mathbf{I})$ by solving the corresponding reverse-time Stochastic Differential Equation (SDE) [36, 37]:

$$d\mathbf{x}_t = \left(f(t, \mathbf{x}_t) - \frac{1+\eta^2}{2} \sigma_t^2 \nabla_{\mathbf{x}} \log p_t(\mathbf{x}_t) \right) dt + \eta \sigma_t d\mathbf{w}_t, \quad (2)$$

where \mathbf{w}_t is a Wiener process, $\nabla_{\mathbf{x}} \log p_t(\mathbf{x}_t)$ is the score, and η controls path stochasticity.

3.2. Rectified Flow

Rectified Flow (RF) [23] is learned via Flow Matching [21], which posits a linear path from $\mathbf{x}_0 \sim \mathcal{N}(\mathbf{0}, \mathbf{I})$ to data \mathbf{x}_1 :

$$\mathbf{x}_t = (1-t)\mathbf{x}_0 + t\mathbf{x}_1, \quad t \in [0, 1]. \quad (3)$$

A velocity field $v_\theta(\mathbf{x}_t, t)$ is trained to approximate $\mathbf{v} = \mathbf{x}_1 - \mathbf{x}_0$. The learned field gives the deterministic probability-flow ODE $d\mathbf{x}_t = v_\theta(\mathbf{x}_t, t) dt$. Following [2, 6, 22], the deterministic flow can be converted into a reverse SDE that maintains consistent marginal distributions:

$$d\mathbf{x}_t = \left(v_\theta(\mathbf{x}_t, t) - \frac{\sigma_t^2}{2} \nabla_{\mathbf{x}} \log p_t(\mathbf{x}_t) \right) dt + \sigma_t d\mathbf{w}_t. \quad (4)$$

3.3. Group Relative Policy Optimization

Group Relative Policy Optimization (GRPO) [35] aligns a pre-trained generator with human preferences using a PPO-style objective [34] and a group-relative advantage. Given a group of G candidates with rewards $\{R_i\}_{i=1}^G$, define $\mu_G = \frac{1}{G} \sum_{j=1}^G R_j$ and $\sigma_G = \sqrt{\frac{1}{G} \sum_{j=1}^G (R_j - \mu_G)^2}$. The normalized advantage is

$$A_i = \frac{R_i - \mu_G}{\sigma_G + \epsilon}, \quad \epsilon > 0, \quad (5)$$

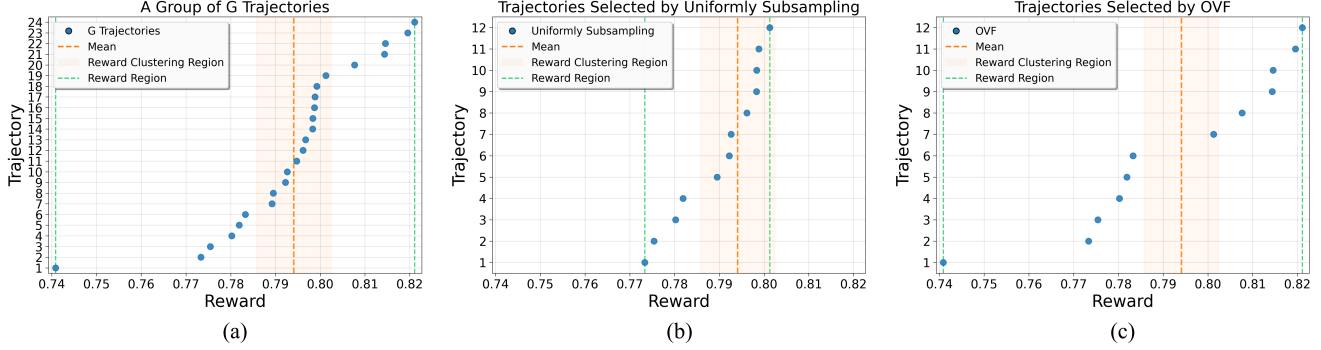


Figure 1. **Reward clustering Phenomenon and OVF effects.** (a) A full group ($G = 24$) exhibits pronounced reward clustering. (b) Uniform subsampling ($k = 12$) preserves the clustering. (c) Our OVF ($k = 12$) alleviates reward clustering by selecting from the reward extremes.

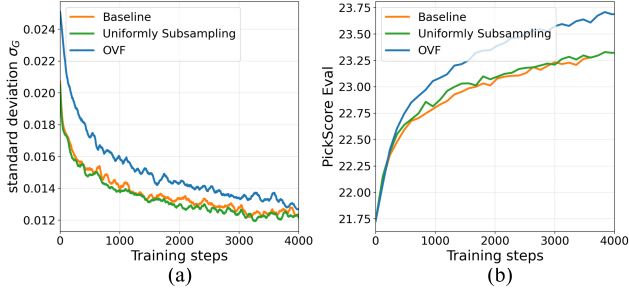


Figure 2. **Visualization of training dynamics on PickScore.** We compare the Baseline ($G = 24$) against Uniform Subsampling ($k = 12$) and our OVF strategy ($k = 12$). (a) Reward standard deviation (σ_G). (b) PickScore Eval.

and the GRPO loss is

$$\mathcal{L}_{\text{GRPO}} = -\mathbb{E}[\min(rA, \text{clip}(r, 1 - \varepsilon, 1 + \varepsilon)A)] + \beta \text{KL}(\pi_\theta \| \pi_{\text{ref}}), \quad (6)$$

where r is the importance ratio between the current and reference policies, ε is the PPO clipping parameter, and β weights the KL regularization toward π_{ref} .

4. Trajectory Analyses of GRPO

4.1. Reward Clustering Phenomenon

The effectiveness of GRPO is closely related to the reward distribution within its sampling group [22]. To resolve the conflict between effectiveness and computational cost, we first examine this distribution empirically.

For a single prompt, we draw a group of G trajectories under the reference policy and compute rewards $\{R_i\}_{i=1}^G$ with group mean μ_G and standard deviation σ_G . As illustrated in Fig. 1 (a), we observe a reward clustering phenomenon: a large fraction of rewards concentrate near μ_G , leading to a small σ_G^2 . We formalize the clustered region by

$$\mathcal{C}_\delta = \{i : |R_i - \mu_G| \leq \delta \sigma_G\}, \quad (7)$$

where $\delta > 0$ controls the neighborhood width.

This clustering induces an attenuation of the advantage signal. For any $i \in \mathcal{C}_\delta$, substituting the advantage definition (Eq. (5)) into (7) yields a mathematical bound

$$|A_i| = \frac{|R_i - \mu_G|}{\sigma_G + \epsilon} \leq \frac{\delta \sigma_G}{\sigma_G + \epsilon} \leq \delta, \quad (8)$$

showing that as the within-group variance σ_G^2 shrinks, the normalized advantage of clustered samples vanishes.

The per-trajectory gradient contribution scales with the advantage,

$$g_i \propto A_i \nabla_\theta \log \pi_\theta(\tau_i). \quad (9)$$

and the mini-batch gradient satisfies $g = \frac{1}{G} \sum_{i=1}^G g_i$. Hence, when $A_i \approx 0$ for many $i \in \mathcal{C}_\delta$, those trajectories contribute negligibly to g despite consuming the same compute.

Finally, a naive solution like uniformly subsampling $k < G$ candidates fails to resolve this. As shown in Fig. 1(b), random subsampling does not increase the variance in expectation; it merely preserves the near-mean concentration. This leaves both the magnitude of A and the effective gradient remain limited.

4.2. Optimal Variance Filtering

Building on the observed reward clustering in Section 4.1, we hypothesize that such clustering is detrimental to optimization. To validate this, we propose Optimal Variance Filtering (OVF), a simple yet effective strategy designed to amplify the advantage signal by maximizing the within-group reward variance. Given rewards $\{R_g\}_{g=1}^G$ and a target size $k < G$, OVF selects the subset

$$\mathcal{K}^* = \arg \max_{\substack{\mathcal{K} \subseteq \{1, \dots, G\} \\ |\mathcal{K}|=k}} \sigma^2(\mathcal{K}). \quad (10)$$

By construction, Eq. (10) prefers subsets that span the reward extremes, thus mitigating the reward clustering phenomenon mentioned in Sec. 4.1.

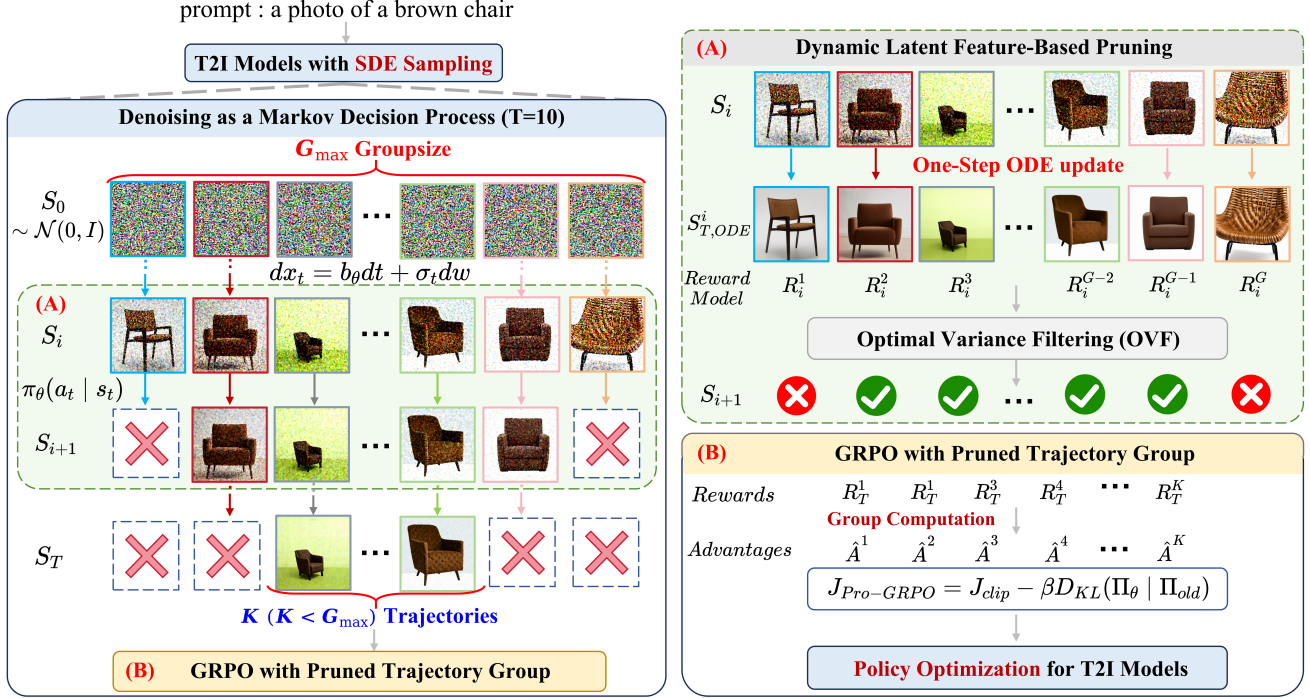


Figure 3. **Overview of the Pro-GRPO.** Pro-GRPO runs a dynamic expand-and-prune schedule inside the T -step denoising. We begin with an expanded group G_{\max} to maximize exploration. At intermediate checkpoints S_i , **(A) Dynamic latent pruning** deterministically projects each active latent to T via a single-step ODE update to obtain a proxy sample and reward \hat{R}_i ; OVF then keeps a high-variance subset and early-terminates the rest (red crosses), progressively narrowing the group to K survivors at S_T . **(B) GRPO on the pruned group** computes group-normalized advantages over the K survivors and updates the policy, achieve high performance with low computational cost.

The effect of OVF is twofold. First, as visualized in Fig. 1 (c), OVF-selected rewards are de-clustered; the distribution spreads toward both tails, confirming the mechanism is effective at mitigating clustering. Second, we evaluate the long-term training impact in Fig. 2. Fig. 2 (a) shows that OVF (blue) consistently maintains a higher reward variance (σ_G) throughout training, while the variance of the Baseline (orange) and Uniform Subsampling (green) groups remains comparatively lower. Fig. 2 (b) demonstrates that training on this OVF-filtered subset ($k < G$) does not just avoid degradation, but outperforms the baseline trained on the full, unfiltered group (G).

This result confirms our “Less is More” hypothesis: a smaller, high-variance subset is not just sufficient, but can outperform a larger, unfiltered group.

5. Pro-GRPO

While OVF demonstrates that maximizing within-group reward variance improves learning, it is inherently a post-sampling filter: reward-clustered trajectories must be fully generated before selection. We therefore introduce Pro-GRPO, a dynamic framework that prunes during sampling. It uses latent features to early-terminate reward-clustered trajectories and employs an “Expand-and-Prune” strategy.

The overall pipeline is shown in Fig. 3.

5.1. Dynamic Pruning Framework

Initialization and multi-step denoising. Given a prompt c , we draw G initial latents $\{\mathbf{x}_0^{(g)}\}_{g=1}^G$ from $\mathcal{N}(\mathbf{0}, \mathbf{I})$ and run reverse-time denoising for T steps. As shown in Section Sec. 3, for both diffusion and rectified flow (RF) models, one reverse-time sampling step admits the unified SDE

$$d\mathbf{x}_t = b_\theta(\mathbf{x}_t, t) dt + \sigma_t d\mathbf{w}_t, \quad (11)$$

where \mathbf{w}_t is a d -dimensional Wiener process and $\sigma_t \geq 0$ controls stochasticity. The drift specializes to each backbone as

$$b_\theta(\mathbf{x}, t) = \begin{cases} f(t, \mathbf{x}) - \frac{1+\eta^2}{2} \sigma_t^2 \nabla_{\mathbf{x}} \log p_t(\mathbf{x}), & \text{Diffusion,} \\ v_\theta(\mathbf{x}, t) - \frac{1}{2} \sigma_t^2 \nabla_{\mathbf{x}} \log p_t(\mathbf{x}), & \text{RF.} \end{cases} \quad (12)$$

With Euler–Maruyama discretization and step size Δt , the g -th trajectory updates as follows, where $\xi_t^{(g)} \sim \mathcal{N}(\mathbf{0}, \mathbf{I})$.

$$\mathbf{x}_{t+\Delta t}^{(g)} = \mathbf{x}_t^{(g)} + b_\theta(\mathbf{x}_t^{(g)}, t) \Delta t + \sigma_t \sqrt{\Delta t} \xi_t^{(g)}. \quad (13)$$

Dynamic Latent Feature-Based Pruning. At pre-specified checkpoints t_i , we cheaply predict the terminal

outcome for each active trajectory by computing a single-step deterministic ODE projection. We use the probability-flow ODE drift

$$b_\theta^{\text{ODE}}(\mathbf{x}, t) = \begin{cases} f(t, \mathbf{x}) - \frac{1}{2}\sigma_t^2 \nabla_{\mathbf{x}} \log p_t(\mathbf{x}), & \text{Diffusion,} \\ v_\theta(\mathbf{x}, t), & \text{RF,} \end{cases} \quad (14)$$

and approximate the ODE terminal preview from $\mathbf{x}_{t_i}^{(g)}$ by one Euler step:

$$\mathbf{x}_{T, \text{ODE}}^{(g)} \approx \mathbf{x}_{t_i}^{(g)} + (T - t_i) b_\theta^{\text{ODE}}(\mathbf{x}_{t_i}^{(g)}, t_i). \quad (15)$$

Next, we pass this preview latent $\mathbf{x}_{T, \text{ODE}}^{(g)}$ through the VAE decoder and the reward model $R(\cdot, c)$ to obtain a proxy reward

$$R_i^{(g)} = R(\mathbf{x}_{T, \text{ODE}}^{(g)}, c). \quad (16)$$

Let K_i denote the number of active trajectories at checkpoint t_i (with $K_1 = G$). Optimal Variance Filtering (OVF) selects a subset $\mathcal{K}_{i+1} \subseteq \{1, \dots, K_i\}$ of size $K_{i+1} < K_i$ that maximizes the within-set reward variance:

$$\mathcal{K}_{i+1} = \arg \max_{\substack{\mathcal{K} \subseteq \{1, \dots, K_i\} \\ |\mathcal{K}| = K_{i+1}}} \frac{1}{K_{i+1}} \sum_{g \in \mathcal{K}} \left(R_i^{(g)} - \mu_{\mathcal{K}} \right)^2. \quad (17)$$

Only trajectories indexed by \mathcal{K}_{i+1} continue denoising after t_i ; the rest are early-terminated and incur no further SDE steps. Repeating this procedure across all checkpoints yields a decreasing sequence of survivor counts $K_1 = G > K_2 > \dots > K_{I+1} = K$.

GRPO with the pruned trajectory set. At terminal time T , we compute final rewards for the survivors $g \in \mathcal{K}_{I+1}$ and calculate the group-normalized advantages:

$$\hat{A}^{(g)} = \frac{R(\mathbf{x}_T^{(g)}, c) - \mu_{\mathcal{K}}}{\sigma_{\mathcal{K}} + \epsilon}, \quad (18)$$

where $\mu_{\mathcal{K}}$ and $\sigma_{\mathcal{K}}$ represent the mean and standard deviation of the rewards $\{R(\mathbf{x}_T^{(h)}, c)\}_{h \in \mathcal{K}_{I+1}}$ within the pruned set.

Let $\mathbf{a}_t^{(g)} = \mathbf{x}_{t+\Delta t}^{(g)} - \mathbf{x}_t^{(g)}$ and $\mathbf{s}_t^{(g)} = (\mathbf{x}_t^{(g)}, t)$. The per-step importance ratio is

$$r_t^{(g)}(\theta) = \frac{\pi_\theta(\mathbf{a}_t^{(g)} | \mathbf{s}_t^{(g)})}{\pi_{\text{old}}(\mathbf{a}_t^{(g)} | \mathbf{s}_t^{(g)})}, \quad (19)$$

where π_θ is the Gaussian policy induced by Eq. (13). We then maximize the Pro-GRPO objective restricted to the surviving trajectories:

$$\begin{aligned} \mathcal{J}_{\text{Pro-GRPO}}(\theta) = \mathbb{E}_c \left[\frac{1}{K} \sum_{g \in \mathcal{K}_{I+1}} \frac{1}{T} \sum_{t=0}^{T-1} \min(r_t^{(g)}(\theta) \hat{A}^{(g)}, \right. \\ \left. \text{clip}(r_t^{(g)}(\theta), 1 - \epsilon, 1 + \epsilon) \hat{A}^{(g)}) \right] - \beta D_{\text{KL}}(\pi_\theta \| \pi_{\text{ref}}). \end{aligned} \quad (20)$$

In this way, Pro-GRPO operates at the optimization cost of a small group of size K , dramatically improving sampling efficiency while enhancing performance.

5.2. Expand and Prune

Leveraging the efficiency of dynamic pruning, Pro-GRPO implements an "Expand-and-Prune" strategy that broadens exploration without incurring prohibitive cost. Instead of starting from a budget-constrained group, Pro-GRPO temporarily expands the initial trajectory pool to a larger size $G_{\text{max}} > K$ to increase coverage of the reward landscape. During generation, pruning is applied in-process: at each checkpoint t_i ($0 < t_1 < \dots < t_I < T$), given K_i active trajectories, OVF (Eq. (10)) selects a high-variance subset \mathcal{K}_{i+1} of size $K_{i+1} < K_i$ to continue, while the rest are early-terminated. Repeating this selection yields a monotone funnel of survivor counts $K_1 = G_{\text{max}} > K_2 > \dots > K_{I+1} = K$. In effect, Pro-GRPO expands the exploration benefits of a large initial group yet keeps the effective integration and optimization cost close to that of the final survivors, thereby delivering superior learning signals under a fixed compute budget.

6. Experiments

6.1. Experimental Setup

Baselines. To demonstrate the applicability of Pro-GRPO, we conduct experiments across two generative paradigms: the diffusion-based Stable Diffusion v1.4 (SD-v1.4) [29] and the flow-based Stable Diffusion 3.5 (SD3.5-M) [8]. We compare our framework against representative RL fine-tuning methods, specifically Flow-GRPO [22] and Dance-GRPO [47]. For a fair comparison, all methods are optimized using standard reward objectives, including HPS-v2.1 [44], CLIP Score [27], and PickScore [16], ensuring that performance gains are attributable to the training strategy rather than the reward signal.

Evaluation Metrics. We evaluate performance on two standard benchmarks: DrawBench [32] and HPSv2 [43]. DrawBench is a benchmark with diverse prompts to evaluate model capabilities, while HPSv2 is designed to evaluate how well generated images align with human preferences. To provide a comprehensive assessment beyond task-specific accuracy, we evaluate the generated images using a suite of metrics, including ImageReward [46], HPS-v2.1 [44], PickScore [16], GenEval [11], and Aesthetic Score [33]. The results of these evaluations, presented in Section 6.2, demonstrate the effectiveness of our Pro-GRPO pipeline in improving both alignment and performance across multiple metrics.

Experimental Settings. We utilize 24 A100 GPUs for flow-based models and 8 A100 GPUs for diffusion-based models. Our configurations are meticulously aligned with

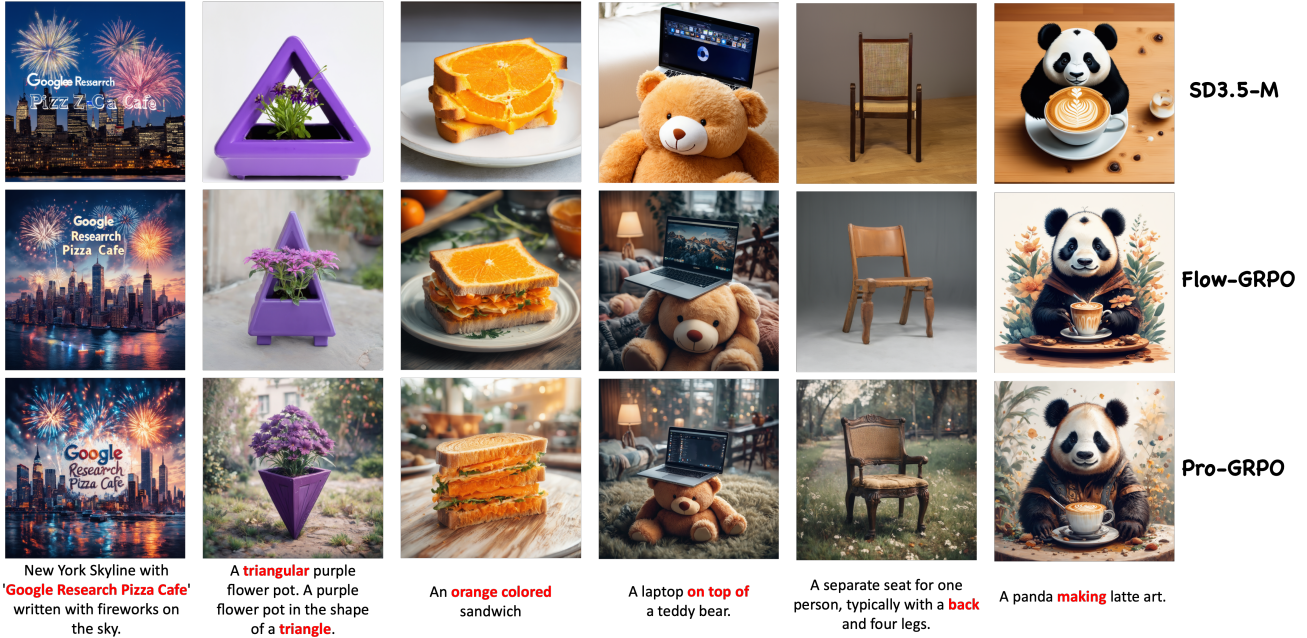


Figure 4. Qualitative comparison between SD3.5-M, Flow-GRPO and Pro-GRPO with PickScore as reward on DrawBench prompts.

Table 1. **Quantitative comparison on flow-based text-to-image generation (SD3.5-Medium)**. We compare Pro-GRPO against the base model and the Flow-GRPO baseline. Note that **Pro-GRPO-Flash** achieves significant speedup while surpassing the baseline, and **Pro-GRPO (Standard)** achieves the best overall performance with moderate acceleration. **Bold** indicates the best result.

Dataset	Model	Efficiency	In-Domain	Out-of-Domain			
		Speedup (\uparrow)	PickScore (\uparrow)	Aes. (\uparrow)	IR (\uparrow)	Pick. (\uparrow)	HPSv2.1 (\uparrow)
DrawBench	SD 3.5-M (Base)	-	-	5.408	0.852	22.425	0.280
	Flow-GRPO	1.00 \times	23.322	5.912	1.298	23.599	0.316
	Pro-GRPO-Flash	1.41\times	23.722	6.030	1.381	23.868	0.319
	Pro-GRPO (Ours)	1.26 \times	24.008	6.046	1.397	24.108	0.322
HPSv2	SD 3.5-M (Base)	-	-	5.868	1.174	22.608	0.308
	Flow-GRPO	1.00 \times	23.322	6.232	1.463	23.899	0.338
	Pro-GRPO-Flash	1.41\times	23.722	6.303	1.495	24.251	0.340
	Pro-GRPO (Ours)	1.26 \times	24.008	6.375	1.509	24.597	0.344

the baselines. Against Flow-GRPO ($G = 24, T = 10$), we evaluate Pro-GRPO (Standard), which expands $G_{\max} = 48$ and prunes at steps $t = \{5, 7\}$ (path: $48 \rightarrow 24 \rightarrow 12$), alongside the efficiency variant Pro-GRPO (Flash) ($G_{\max} = 24$, path: $24 \rightarrow 16 \rightarrow 12$). Against DanceGRPO ($G = 16, T = 50$), we adapt our schedule to start with $G_{\max} = 48$ and prune at $t = \{30, 40\}$ (path: $48 \rightarrow 32 \rightarrow 8$). Full configurations are detailed in the Appendix.

6.2. Main Results

Performance on flow-based models. Table 1 demonstrates that Pro-GRPO improves both optimization objectives and out-of-domain (OOD) metrics while reducing

training costs. On DrawBench, Pro-GRPO consistently outperforms the baseline Flow-GRPO across all metrics with a PickScore of 24.008 (+0.686) and Aesthetic score of 6.046 (+0.134). Notably, as shown in the ‘Efficiency’ column, this performance gain is achieved alongside a 1.26 \times training speedup, attributed to the reduced group size during optimization. This advantage extends to HPSv2, as reflected in OOD metrics like ImageReward (1.509 vs. 1.463). The efficiency benefits are particularly evident in the lightweight Pro-GRPO-Flash ($G_{\max} = 24 \rightarrow 12$). It delivers a 1.41 \times speedup while still surpassing the baseline on DrawBench (23.722 vs. 23.322). This result isolates the benefit of in-process pruning, supporting our “less-is-more” hypothesis.

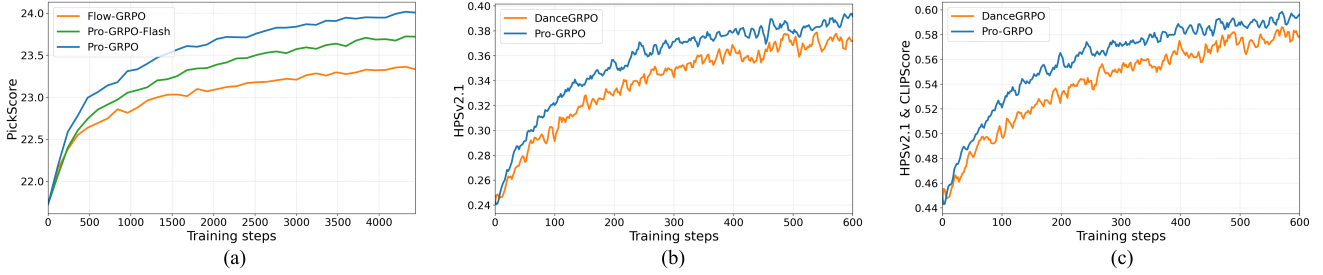


Figure 5. **Training dynamics.** Reward trajectories during optimization. (a) **Flow-based (SD3.5, PickScore)**: Pro-GRPO (blue) and Pro-GRPO-Flash (green) converge faster and reach higher plateaus than Flow-GRPO (orange). (b) **Diffusion-based (SD-v1.4, HPSv2.1)**: Pro-GRPO consistently outperforms DanceGRPO throughout training. (c) **Diffusion-based (SD-v1.4, HPSv2.1 & CLIP)**: Pro-GRPO maintains a stable margin, indicating stronger multi-objective optimization.

Table 2. **Quantitative comparison on diffusion-based T2I generation (SD-v1.4).** We compare Pro-GRPO against DanceGRPO under single-objective (HPSv2.1) and multi-objective (HPSv2.1 & CLIP) rewards. “In-Domain” refers to the metric used during optimization (HPSv2.1 & CLIP), while “Out-of-Domain” metrics assess generalization. **Bold** indicates the best performance.

Dataset	Model	In-Domain		Out-of-Domain			
		HPSv2.1 (\uparrow)	CLIP (\uparrow)	Aes. (\uparrow)	IR (\uparrow)	Pick. (\uparrow)	HPSv2.1 (\uparrow)
DrawBench	SD v1.4 (Base)	-	-	5.207	-0.029	21.084	0.2445
	DanceGRPO (HPS)	0.369	-	5.766	0.884	21.903	0.3250
	Pro-GRPO (HPS)	0.391	-	5.894	0.933	21.896	0.3390
	DanceGRPO (HPS+CLIP)	0.575	-	5.821	0.835	21.875	0.3230
	Pro-GRPO (HPS+CLIP)	0.596	-	5.897	0.974	22.073	0.3390
HPSv2	SD v1.4 (Base)	-	-	5.389	0.015	20.688	0.2390
	DanceGRPO (HPS)	0.369	-	6.229	1.079	22.127	0.3660
	Pro-GRPO (HPS)	0.391	-	6.253	1.114	22.202	0.3830
	DanceGRPO (HPS+CLIP)	0.575	-	6.212	1.057	22.102	0.3670
	Pro-GRPO (HPS+CLIP)	0.596	-	6.273	1.140	22.271	0.3800

Complementing these metrics, Fig. 5 (a) shows faster convergence and a higher asymptote. Together with the qualitative comparisons in Fig. 4, these findings indicate that Pro-GRPO improves sample efficiency and robustness without overfitting.

Performance on diffusion-based models. Table 2 and Fig. 5 (b,c) present the comparison against DanceGRPO. In the single-objective setting (HPSv2.1), Pro-GRPO demonstrates enhanced optimization capability, surpassing DanceGRPO in in-domain rewards (0.391 vs. 0.369) and consistently improving OOD metrics (e.g., ImageReward on HPSv2: 1.114 vs. 1.079). This is mirrored in Fig. 5(b) by a faster rise and higher asymptote. In the multi-objective setting (HPSv2.1 + CLIP), the advantage of our approach is also pronounced. Pro-GRPO achieves the best OOD results across the board on both datasets. Fig. 5 (c) shows a stable margin throughout training on the composite objective. These findings support our core insight: a small, high-variance survivor set provides a stronger learning signal than the full, unfiltered group.

Semantic alignment and compositionality. We assess text–image grounding on GenEval (Table 3), which is not used for training (all models are tuned only with PickScore). Pro-GRPO surpasses Flow-GRPO on the Overall score (0.726 vs. 0.719) and on every fine-grained category: Two-Obj. (0.947 vs. 0.942), Colors (0.867 vs. 0.851), Position (0.323 vs. 0.288, +0.035). The strongest gain on Position indicates improved spatial reasoning and compositional binding, suggesting that variance-aware pruning produces trajectories that carry clearer semantic signals. The consistent improvements on this unseen benchmark further support that Pro-GRPO enhances semantic alignment without reward-specific overfitting.

Computational efficiency analysis. To quantify the cost-effectiveness of Pro-GRPO, we use calcflops [45] to profile per-call FLOPs and the cost of a full sampling–training cycle (Table 4). Pro-GRPO reallocates compute from uniform training on a fixed group to exploration and selection. It briefly expands the initial pool (G_{\max}) and prunes in-process, early-terminating reward-clustered trajectories

Table 3. **Quantitative evaluation on GenEval benchmark.** All models are fine-tuned using the PickScore reward. We report the Overall score and fine-grained accuracies.

Model	Overall Score (\uparrow)	Fine-grained Accuracy		
		Two Obj.	Colors	Position
SD 3.5-M (Base)	0.696	0.869	0.817	0.248
Flow-GRPO	0.719	0.942	0.851	0.288
Pro-GRPO	0.726	0.947	0.867	0.323

Table 4. **Computational efficiency analysis.** We report the FLOPs (in Tera) and relative speedup. The top section lists the cost of atomic operations. The bottom section compares the total computational cost of a full epoch, including trajectory sampling and policy optimization. Pro-GRPO reduces the aggregate FLOPs by early-terminating reward-clustered trajectories during the sampling phase.

Component / Method	FLOPs (T) \downarrow	Speedup \uparrow
<i>Atomic Operations (Per Call)</i>		
Noise Prediction	3.88	–
VAE Decoding	2.49	–
Reward Computation	0.34	–
<i>Full Training Framework</i>		
Flow-GRPO (Baseline)	453474.18	1.00 \times
Pro-GRPO (Standard)	335626.82	1.26\times
Pro-GRPO (Flash)	267365.79	1.41\times

to avoid their remaining denoising steps. Because only the survivor set K proceeds to backprop, the optimization cost scales with K rather than G_{\max} . This yields substantial savings. FLOPs drop from 453474 T (Flow-GRPO) to 335627 T with Pro-GRPO Standard (–26%, 1.26 \times speedup), and to 267366 T with Pro-GRPO Flash (–41%, 1.41 \times). The performance in Table 1 shows that investing compute in exploration and variance-based pruning is more effective and more efficient than uniformly training on a large, unfilter group. The detailed calculation procedure is provided in the appendix.

6.3. Ablation Studies

Effect of Initial Group Size. Table 5 investigates the impact of the initial group size G_{\max} on performance. By fixing the final survivor set $K = 8$ and scaling G_{\max} from 32 to 64, we observe a consistent improvement across all metrics by exposing superior candidates for OVF. We also observe a trend of diminishing rewards: the performance gains taper off at larger scales (e.g., 48 \rightarrow 64). The Out-of-Domain HPSv2.1 score plateaus at 0.383, indicating that the marginal informational value of additional trajectories saturates. This suggests that scaling G_{\max} indefinitely yields limited benefits beyond a sufficiency threshold. Be-

Table 5. **Ablation study on scaling initial group size (G_{\max}).** Experiments are conducted on SD1.4 optimized with HPSv2.1.

Pruning Path ($G_{\max} \rightarrow K$)	In-Domain	Out-of-Domain			
	HPSv2.1	Aes.	IR	Pick.	HPSv2.1
32 \rightarrow 8	0.386	6.327	1.080	22.075	0.379
48 \rightarrow 8	0.391	6.253	1.114	22.202	0.383
64 \rightarrow 8	0.393	6.350	1.120	22.231	0.383

Table 6. **Ablation study on pruning checkpoints.** Experiments are conducted on SD-v1.4 ($T = 50$) optimized with HPSv2.1, using a pruning path of 32 \rightarrow 8.

Pruning Steps (t_1, t_2)	In-Domain	Out-of-Domain			
	HPSv2.1	Aes.	IR	Pick.	HPSv2.1
10, 20	0.373	6.132	1.016	21.711	0.364
20, 30	0.382	6.160	1.063	21.859	0.369
30, 40 (Ours)	0.391	6.327	1.080	22.075	0.379

cause Pro-GRPO prunes in-process, the effective optimization cost remains tied to K rather than G_{\max} , enabling us to exploit larger initial group size without proportional compute growth.

Effect of Pruning Timesteps. Table 6 examines where to place pruning checkpoints under $T=50$ with a path 32 \rightarrow 8. The results show that OVF-based pruning is effective across schedules; even an early schedule {10, 20} yields gains. Shifting the checkpoints deeper improves accuracy, with {30, 40} attaining the best trade-off. For example, in-domain HPSv2.1 rises from 0.373 to 0.391, and OOD PickScore from 21.711 to 22.075. The pattern suggests that an early checkpoint can remove clear low-value samples for compute savings, while a later checkpoint refines the survivor set once latents carry richer semantics.

7. Conclusion

In this work, we address the computational bottleneck in GRPO caused by the conflict between large group sizes and cost. Identifying a "Reward Clustering Phenomenon" that dilutes advantage signals, we initially explored Optimal Variance Filtering (OVF). While OVF confirms that small, high-variance subsets are superior, its post-sampling nature incurs overhead. Consequently, we propose Pro-GRPO, a framework shifting to proactive, in-process pruning. By leveraging latent features to early-terminate redundant samples, Pro-GRPO's "Expand-and-Prune" strategy decouples exploration breadth from optimization cost. Experiments on diffusion and flow-based models demonstrate significantly enhanced alignment performance and efficiency.

References

- [1] Michael Samuel Albergo and Eric Vanden-Eijnden. Building normalizing flows with stochastic interpolants. In *The Eleventh International Conference on Learning Representations*, 2023. 2
- [2] Michael S Albergo, Nicholas M Boffi, and Eric Vanden-Eijnden. Stochastic interpolants: A unifying framework for flows and diffusions. *arXiv preprint arXiv:2303.08797*, 2023. 2
- [3] James Betker, Gabriel Goh, Li Jing, Tim Brooks, Jianfeng Wang, Linjie Li, Long Ouyang, Juntang Zhuang, Joyce Lee, Yufei Guo, et al. Improving image generation with better captions. *Computer Science*. <https://cdn.openai.com/papers/dall-e-3.pdf>, 2(3):8, 2023. 2
- [4] Kevin Black, Michael Janner, Yilun Du, Ilya Kostrikov, and Sergey Levine. Training diffusion models with reinforcement learning. *arXiv preprint arXiv:2305.13301*, 2023. 1
- [5] Yuanjiang Cao, Quan Z Sheng, Julian McAuley, and Lina Yao. Reinforcement learning for generative ai: A survey. *arXiv preprint arXiv:2308.14328*, 2023. 1
- [6] Carles Domingo-Enrich, Michal Drozdal, Brian Karrer, and Ricky T. Q. Chen. Adjoint matching: Fine-tuning flow and diffusion generative models with memoryless stochastic optimal control. In *The Thirteenth International Conference on Learning Representations*, 2025. 2
- [7] Chengqi Duan, Rongyao Fang, Yuqing Wang, Kun Wang, Linjiang Huang, Xingyu Zeng, Hongsheng Li, and Xihui Liu. Got-r1: Unleashing reasoning capability of mllm for visual generation with reinforcement learning. *CoRR*, abs/2505.17022, 2025. 1
- [8] Patrick Esser, Sumith Kulal, Andreas Blattmann, Rahim Entezari, Jonas Müller, Harry Saini, Yam Levi, Dominik Lorenz, Axel Sauer, Frederic Boesel, Dustin Podell, Tim Dockhorn, Zion English, and Robin Rombach. Scaling rectified flow transformers for high-resolution image synthesis. In *Forty-first International Conference on Machine Learning*, 2024. 2, 5
- [9] Matteo Gallici and Haitz Sáez de Ocariz Borde. Fine-tuning next-scale visual autoregressive models with group relative policy optimization. In *2nd Workshop on Models of Human Feedback for AI Alignment*, 2025. 2
- [10] Ruiqi Gao, Emiel Hoogeboom, Jonathan Heek, Valentin De Bortoli, Kevin Patrick Murphy, and Tim Salimans. Diffusion models and gaussian flow matching: Two sides of the same coin. In *The Fourth Blogpost Track at ICLR 2025*, 2025. 2
- [11] Dhruva Ghosh, Hannaneh Hajishirzi, and Ludwig Schmidt. Geneval: An object-focused framework for evaluating text-to-image alignment. *Advances in Neural Information Processing Systems*, 36:52132–52152, 2023. 5
- [12] Ziyu Guo, Renrui Zhang, Chengzhuo Tong, Zhizheng Zhao, Rui Huang, Haoquan Zhang, Manyuan Zhang, Jiaming Liu, Shanghang Zhang, Peng Gao, et al. Can we generate images with cot? let’s verify and reinforce image generation step by step. *arXiv preprint arXiv:2501.13926*, 2025. 1, 2
- [13] Xiaoxuan He, Siming Fu, Yuke Zhao, Wanli Li, Jian Yang, Dacheng Yin, Fengyun Rao, and Bo Zhang. Tempflow-grpo: When timing matters for grpo in flow models, 2025. 2
- [14] Jonathan Ho, Ajay Jain, and Pieter Abbeel. Denoising diffusion probabilistic models. *Advances in neural information processing systems*, 33:6840–6851, 2020. 2
- [15] Zijing Hu, Fengda Zhang, Long Chen, Kun Kuang, Jiahui Li, Kaifeng Gao, Jun Xiao, Xin Wang, and Wenwu Zhu. Towards better alignment: Training diffusion models with reinforcement learning against sparse rewards. In *Proceedings of the Computer Vision and Pattern Recognition Conference*, pages 23604–23614, 2025. 1
- [16] Yuval Kirstain, Adam Polyak, Uriel Singer, Shahbuland Matiana, Joe Penna, and Omer Levy. Pick-a-pic: An open dataset of user preferences for text-to-image generation. *Advances in neural information processing systems*, 36:36652–36663, 2023. 5
- [17] Black Forest Labs, Stephen Batifol, Andreas Blattmann, Frederic Boesel, and Saksham Consul et al. Flux.1 kontext: Flow matching for in-context image generation and editing in latent space, 2025. 2
- [18] Junzhe Li, Yutao Cui, Tao Huang, Yinping Ma, Chun Fan, Miles Yang, and Zhao Zhong. Mixgrpo: Unlocking flow-based grpo efficiency with mixed ode-sde. *arXiv preprint arXiv:2507.21802*, 2025. 2
- [19] Yuming Li, Yikai Wang, Yuying Zhu, Zhongyu Zhao, Ming Lu, Qi She, and Shanghang Zhang. Branchgrpo: Stable and efficient grpo with structured branching in diffusion models, 2025. 2
- [20] Zejian Li, Yize Li, Chenye Meng, Zhongni Liu, Ling Yang, Shengyuan Zhang, Guang Yang, Changyuan Yang, Zhiyuan Yang, and Lingyun Sun. Inversion-dpo: Precise and efficient post-training for diffusion models. In *Proceedings of the 33rd ACM International Conference on Multimedia*, pages 9901–9910, 2025. 1
- [21] Yaron Lipman, Ricky T. Q. Chen, Heli Ben-Hamu, Maximilian Nickel, and Matthew Le. Flow matching for generative modeling. In *The Eleventh International Conference on Learning Representations*, 2023. 2
- [22] Jie Liu, Gongye Liu, Jiajun Liang, Yangguang Li, Jiaheng Liu, Xintao Wang, Pengfei Wan, Di Zhang, and Wanli Ouyang. Flow-grpo: Training flow matching models via online rl. *arXiv preprint arXiv:2505.05470*, 2025. 1, 2, 3, 5
- [23] Xingchao Liu, Chengyue Gong, and Qiang Liu. Flow straight and fast: Learning to generate and transfer data with rectified flow. *arXiv preprint arXiv:2209.03003*, 2022. 2
- [24] Xiaoxiao Ma, Haibo Qiu, Guohui Zhang, Zhixiong Zeng, Siqi Yang, Lin Ma, and Feng Zhao. Stage: Stable and generalizable grpo for autoregressive image generation, 2025. 2
- [25] Zichen Miao, Jiang Wang, Ze Wang, Zhengyuan Yang, Lijuan Wang, Qiang Qiu, and Zicheng Liu. Training diffusion models towards diverse image generation with reinforcement learning. In *Proceedings of the IEEE/CVF Conference on Computer Vision and Pattern Recognition*, pages 10844–10853, 2024. 1
- [26] Dustin Podell, Zion English, Kyle Lacey, Andreas Blattmann, Tim Dockhorn, Jonas Müller, Joe Penna, and Robin Rombach. Sd-xl: Improving latent diffusion models for high-resolution image synthesis, 2023. 2
- [27] Alec Radford, Jong Wook Kim, Chris Hallacy, Aditya Ramesh, Gabriel Goh, Sandhini Agarwal, Girish Sastry,

- Amanda Askell, Pamela Mishkin, Jack Clark, et al. Learning transferable visual models from natural language supervision. In *International conference on machine learning*, pages 8748–8763. PmLR, 2021. 5
- [28] Rafael Rafailov, Archit Sharma, Eric Mitchell, Christopher D Manning, Stefano Ermon, and Chelsea Finn. Direct preference optimization: Your language model is secretly a reward model. In *Advances in Neural Information Processing Systems*, pages 53728–53741. Curran Associates, Inc., 2023. 1
- [29] Robin Rombach, Andreas Blattmann, Dominik Lorenz, Patrick Esser, and Björn Ommer. High-resolution image synthesis with latent diffusion models. In *Proceedings of the IEEE/CVF conference on computer vision and pattern recognition*, pages 10684–10695, 2022. 5
- [30] Nataniel Ruiz, Yuanzhen Li, Varun Jampani, Yael Pritch, Michael Rubinstein, and Kfir Aberman. Dreambooth: Fine tuning text-to-image diffusion models for subject-driven generation. In *CVPR*, pages 22500–22510, 2023. 2
- [31] Chitwan Saharia, William Chan, Saurabh Saxena, Lala Li, Jay Whang, Emily L Denton, Kamyar Ghasemipour, Raphael Gontijo Lopes, Burcu Karagol Ayan, Tim Salimans, Jonathan Ho, David J Fleet, and Mohammad Norouzi. Photorealistic text-to-image diffusion models with deep language understanding. In *Advances in Neural Information Processing Systems*, pages 36479–36494. Curran Associates, Inc., 2022. 2
- [32] Chitwan Saharia, William Chan, Saurabh Saxena, Lala Li, Jay Whang, Emily L Denton, Kamyar Ghasemipour, Raphael Gontijo Lopes, Burcu Karagol Ayan, Tim Salimans, et al. Photorealistic text-to-image diffusion models with deep language understanding. *Advances in neural information processing systems*, 35:36479–36494, 2022. 5
- [33] Christoph Schuhmann. Laion aesthetics. <https://laion.ai/blog/laion-aesthetics/>, 2022. Accessed: 2022-08. 5
- [34] John Schulman, Filip Wolski, Prafulla Dhariwal, Alec Radford, and Oleg Klimov. Proximal policy optimization algorithms. *arXiv preprint arXiv:1707.06347*, 2017. 1, 2
- [35] Zhihong Shao, Peiyi Wang, Qihao Zhu, Runxin Xu, Junxiao Song, Mingchuan Zhang, Y. K. Li, Y. Wu, and Daya Guo. Deepseekmath: Pushing the limits of mathematical reasoning in open language models. *CoRR*, abs/2402.03300, 2024. 1, 2
- [36] Yang Song and Stefano Ermon. Generative modeling by estimating gradients of the data distribution. *Advances in neural information processing systems*, 32, 2019. 2
- [37] Yang Song, Jascha Sohl-Dickstein, Diederik P Kingma, Abhishek Kumar, Stefano Ermon, and Ben Poole. Score-based generative modeling through stochastic differential equations. In *International Conference on Learning Representations*, 2021. 2
- [38] Bram Wallace, Meihua Dang, Rafael Rafailov, Linqi Zhou, Aaron Lou, Senthil Purushwalkam, Stefano Ermon, Caiming Xiong, Shafiq Joty, and Nikhil Naik. Diffusion model alignment using direct preference optimization. In *Proceedings of the IEEE/CVF Conference on Computer Vision and Pattern Recognition*, pages 8228–8238, 2024. 1
- [39] Junke Wang, Zhi Tian, Xun Wang, Xinyu Zhang, Weilin Huang, Zuxuan Wu, and Yu-Gang Jiang. Simplear: Pushing the frontier of autoregressive visual generation through pre-training, sft, and rl. *arXiv preprint arXiv:2504.11455*, 2025. 2
- [40] Yibin Wang, Zhimin Li, Yuhang Zang, Yujie Zhou, Jiazi Bu, Chunyu Wang, Qinglin Lu, Cheng Jin, and Jiaqi Wang. Prefgrpo: Pairwise preference reward-based grpo for stable text-to-image reinforcement learning, 2025. 2
- [41] Chenfei Wu, Jiahao Li, Jingren Zhou, Junyang Lin, Kaiyuan Gao, and Kun Yan et al. Qwen-image technical report, 2025. 2
- [42] Mingrui Wu, Lu Wang, Pu Zhao, Fangkai Yang, Jianjin Zhang, Jianfeng Liu, Yuefeng Zhan, Weihao Han, Hao Sun, Jiayi Ji, et al. Reprompt: Reasoning-augmented reprompting for text-to-image generation via reinforcement learning. *arXiv preprint arXiv:2505.17540*, 2025. 1
- [43] Xiaoshi Wu, Yiming Hao, Keqiang Sun, Yixiong Chen, Feng Zhu, Rui Zhao, and Hongsheng Li. Human preference score v2: A solid benchmark for evaluating human preferences of text-to-image synthesis. *CoRR*, abs/2306.09341, 2023. 5
- [44] Xiaoshi Wu, Keqiang Sun, Feng Zhu, Rui Zhao, and Hongsheng Li. Better aligning text-to-image models with human preference. *arXiv preprint arXiv:2303.14420*, 1(3), 2023. 5
- [45] xiaojue ye. calfllops: a flops and params calculate tool for neural networks in pytorch framework, 2023. 7
- [46] Jiazheng Xu, Xiao Liu, Yuchen Wu, Yuxuan Tong, Qinkai Li, Ming Ding, Jie Tang, and Yuxiao Dong. Imagereward: Learning and evaluating human preferences for text-to-image generation. *Advances in Neural Information Processing Systems*, 36:15903–15935, 2023. 5
- [47] Zeyue Xue, Jie Wu, Yu Gao, Fangyuan Kong, Lingting Zhu, Mengzhao Chen, Zhiheng Liu, Wei Liu, Qiushan Guo, Weilin Huang, et al. Dancegrpo: Unleashing grpo on visual generation. *arXiv preprint arXiv:2505.07818*, 2025. 1, 2, 5
- [48] Shihao Yuan, Yahui Liu, Yang Yue, Jingyuan Zhang, Wangmeng Zuo, Qi Wang, Fuzheng Zhang, and Guorui Zhou. Argrpo: Training autoregressive image generation models via reinforcement learning. *arXiv preprint arXiv:2508.06924*, 2025. 2
- [49] Yu Zhang, Yunqi Li, Yifan Yang, Rui Wang, Yuqing Yang, Dai Qi, Jianmin Bao, Dongdong Chen, Chong Luo, and Lili Qiu. Reasongen-r1: Cot for autoregressive image generation models through sft and rl. *arXiv preprint arXiv:2505.24875*, 2025. 2